Electronic Supplementary Information (ESI)

ATRP Catalysts of Tetradentate Guanidine Ligands – Do Guanidine Donors Induce a Faster Atom Transfer?

Konstantin W. Kröckert,[a] Felix Garg,[a] Joshua Heck,[a] Michel V. Heinz,[a] Justin Lange,[a] Regina Schmidt,[a] Alexander Hoffmann[a] and Sonja Herres-Pawlis*[a]

Table of Contents

[a] *Institute of Inorganic Chemistry, RWTH Aachen University, Landoltweg 1a, 52074 Aachen (Germany). E-mail: sonja.herres-pawlis@ac.rwth-aachen.de*

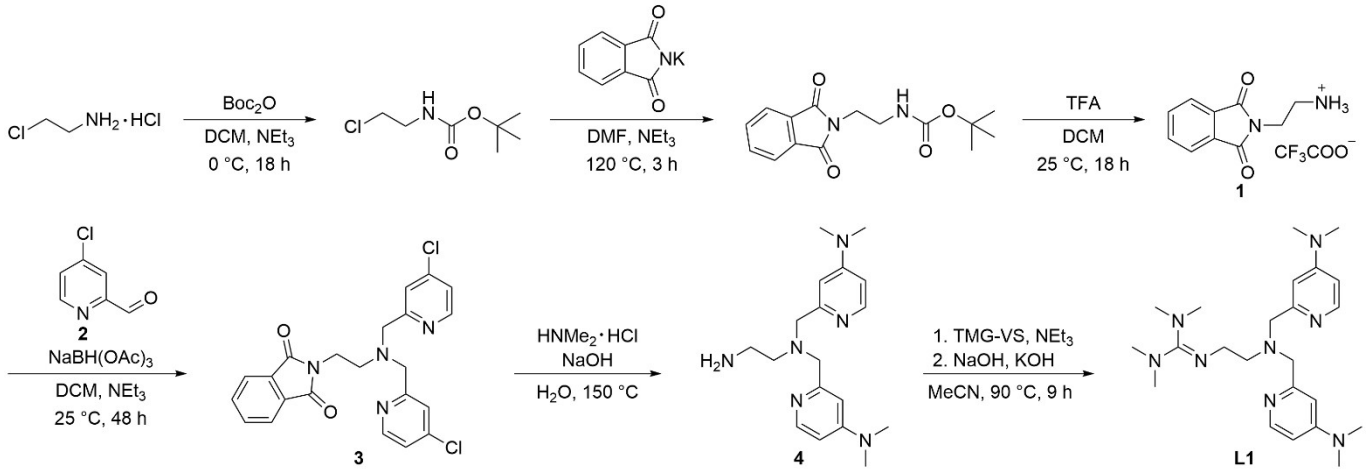

Scheme S1: Synthetic route to the ligand TMG-4NMe$_2$uns-penp (**L1**).

Synthesis of L1

Resynthesis of *tert*-Butyl(2-chloroethyl)carbamate[1]

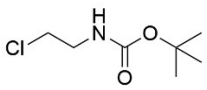

2-Chloroethylamine hydrochloride (15.0 g, 129 mmol, 1 eq.) and NEt_3 (13.1 g, 129 mmol, 1 eq.) were dissolved in DCM (200 mL). Boc_2O (28.2 g, 129 mmol, 1 eq.) was added at 0 °C and the solution was stirred for 18 h. After washing with water the organic phase was dried over Na_2SO_4 and the solvent was removed under reduced pressure (Yield = 95 %, 22.0 g, 123 mmol). ^{1}H NMR (400 MHz, $CDCl_3$): δ = 4.95 (br. s, 1H), 3.59 (t, J = 5.6 Hz, 2H), 3.46 (q, J = 5.4 Hz, 2H), 1.44 (s, 9H) ppm. Additional information on the synthesis of the target compound and original analysis data files are available via Chemotion Repository: https://dx.doi.org/10.14272/reaction/SA-FUHFF-UHFFFADPSC-VACLTXTYDF-UHFFFADPSC-NUHFF-NUHFF-NUHFF-ZZZ

Resynthesis of *tert*-Butyl(2-(1,3-dioxoisoindolin-2-yl)ethyl)carbamate[2,3]

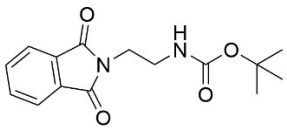

tert-Butyl(2-chloroethyl)carbamate (22.0 g, 123 mmol, 1 eq.) and potassium phthalimide (22.7 g, 122.6 mmol, 1 eq.) were dissolved in DMF (250 mL). The solution was stirred for 3 h at 120 °C and after cooling to room temperature it was poured into water (600 mL). The white precipitate was washed with water, solved in DCM (200 mL) and washed again with water (1 x 200 mL). The organic phase was dried over Na_2SO_4 and the solvent was removed under reduced pressure (Yield = 88 %, 31.3 g, 108 mmol). ^{1}H NMR (400 MHz, $CDCl_3$): δ = 7.87 – 7.83 (m, 2H), 7.74 – 7.69 (m, 2H), 4.82 (br. s, 1H), 3.83 (dd, J = 6.3, 5.0 Hz, 2H), 3.49 – 3.36 (m, 2H), 1.34 (s, 9H) ppm. Additional information on the synthesis of the target compound and original analysis data files are available via Chemotion Repository: https://dx.doi.org/10.14272/reaction/SA-FUHFF-UHFFFADPSC-ZBUIOQQRBI-UHFFFADPSC-NUHFF-NUHFF-NUHFF-ZZZ

Resynthesis of 2-(1,3-Dioxoisoindolin-2-yl)ethan-1-aminium 2,2,2-trifluoroacetate[3]

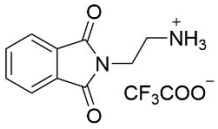

tert-Butyl(2-(1,3-dioxoisoindolin-2-yl)ethyl)carbamate (31.3 g, 108 mmol, 1 eq.) was diluted in DCM (100 mL). TFA (207 mL, 2.70 mol, 25 eq.) was added and the reaction mixture was stirred for 18 h at 25 °C. The solvent and residual TFA were removed under reduced pressure to yield a yellow oil. It was dissolved in DCM (5 mL) and slowly added to a stirred mixture of 200 mL Et_2O and hexane (1/1) which results in precipitated product (Yield = 91 %, 30.0 g, 98.6 mmol). ^{1}H NMR (400 MHz, DMSO-d_6): δ = 7.96 – 7.77 (m, 7H), 3.84 (t, J = 5.9 Hz, 2H), 3.09 (t, J = 5.9 Hz, 2H) ppm. Additional information on the synthesis of the target compound and original analysis data files are available via Chemotion Repository: https://dx.doi.org/10.14272/reaction/SA-FUHFF-UHFFFADPSC-MGKZRLPYSB-UHFFFADPSC-NUHFF-NUHFF-NUHFF-ZZZ

Resynthesis of 4-Chloropicolinaldehyde[4]

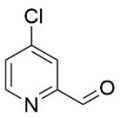

Activated MnO_2 (57.29 g, 659.0 mmol, 12.4 eq.) was suspended in $CHCl_3$ (95 mL) and (4-chloropyridin-2-yl)methanol (7.63 g, 53.15 mmol, 1 eq.) was added. The suspension was refluxed for 2 h, was hot filtered over Celite on a glass filter and washed with $CHCl_3$. The solvent was evaporated under reduced pressure to receive the product (Yield = 64 %, 4.83 g, 34.1 mmol). ^{1}H NMR (400 MHz, $CDCl_3$): δ = 10.05 (s, 1H), 8.69 (d, J = 5.0 Hz, 1H), 7.94 (d, J = 1.5 Hz, 1H), 7.52 (dd, J = 5.0, 1.5 Hz, 1H) ppm. Additional information on the synthesis of the target compound

and original analysis data files are available via Chemotion Repository: https://dx.doi.org/10.14272/reaction/SA-FUHFF-UHFFFADPSC-NZLNQSUMFS-UHFFFADPSC-NUHFF-NUHFF-NUHFF-ZZZ

Cristallographic Data and Parameters

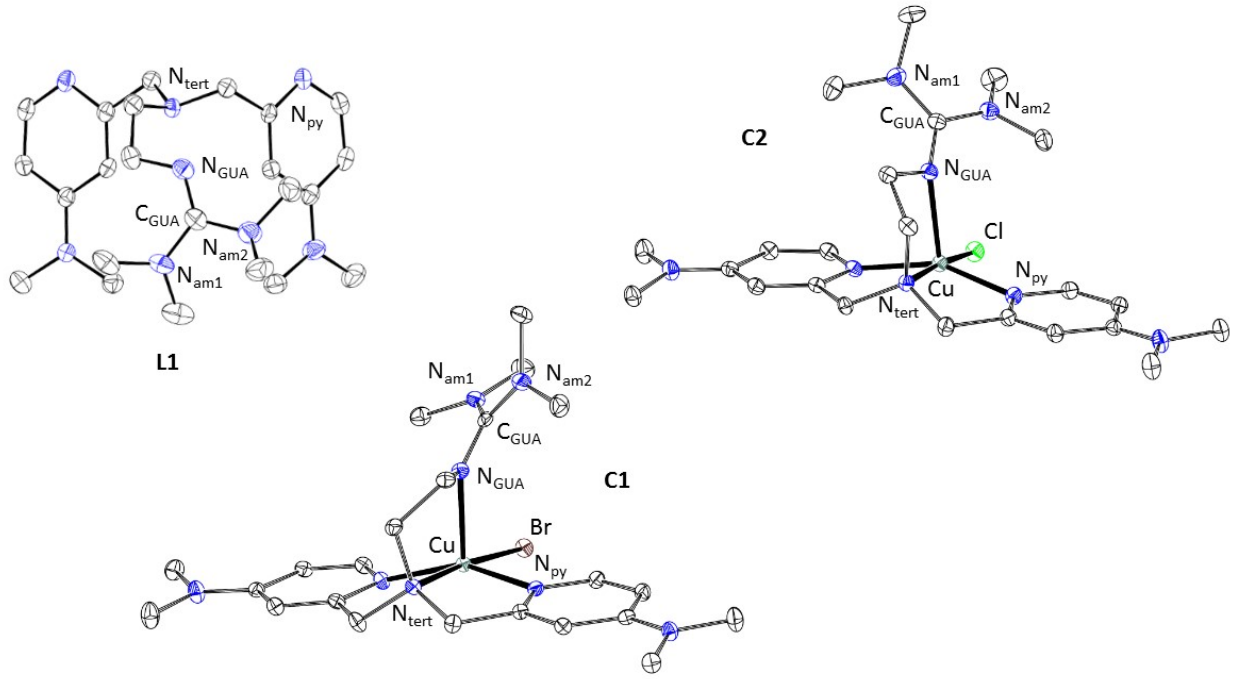

Fig. S1: Molecular structure of the ligand **L1** or of the cationic complex units of [Cu(TMG-4NMe$_2$uns-penp)Br]Br (**C1**) and [Cu(TMG-4NMe$_2$uns-penp)Cl]Cl (**C2**) in the solid state (ellipsoids drawn at the 50% probability level). H atoms, not coordinating anions and solvent molecules are omitted for clarity.

Table S1: Crystallographic data and parameters of the ligand **L1** and Cu(II) complexes **C1** and **C2**.

Complex/Ligand	**L1**	**C1**	**C2**
Empirical formula	$C_{23}H_{33}N_8$	$C_{23}H_{38}Br_2CuN_8$	$C_{23}H_{38}Cl_2CuN_8$
Formula mass [g mol^{-1}]	426.61	649.97	561.05
Crystal size [mm]	0.25 x 0.20 x 0.18	0.21 x 0.18 x 0.14	0.16 x 0.14 x 0.10
T [K]	100(2)	100(2)	100(2)
Crystal system	Triclinic	Monoclinic	Monoclinic
Space group	$P\bar{1}$	$P2_1/n$	$P2_1/n$
a [Å]	8.624(3)	8.4759(17)	8.2624(17)
b [Å]	9.128(3)	22.426(5)	22.189(4)
c [Å]	15.701(5)	14.174(3)	14.293(3)
α [°]	76.082(6)	90	90
β [°]	85.831(6)	95.99(3)	95.53(3)
γ [°]	77.379(6)	90	90
V [Å^3]	1170.6(6)	2679.6(9)	2608.2(9)
Z	2	4	4
$\rho_{calcd.}$ [g cm^{-3}]	1.210	1.611	1.429
μ [mm^{-1}]	0.076	3.825	1.071
λ [Å]	0.71073	0.71073	0.71073
F(000)	464	1324	1180
hkl range	-10/10, -11/11, -18/18	-10/9, -19/27, -17/16	-8/12, -33/33, -19/21
Reflections collected	13304	29466	67965
Independent reflections	4333	4973	9614
$R_{int.}$	0.0913	0.0228	0.0676
No. parameters	289	315	315
R_1 [I ≥ 2σ(*I*)]	0.0573	0.03082	0.0309
wR_2 (all data)	0.1352	0.0651	0.0780
Goodness-of-fit	0.934	1.271	0.944
$\Delta\rho_{fin}$ max/min [eÅ^{-3}]	0.237/-0.227	1.078/-0.715	0.455/-0.480

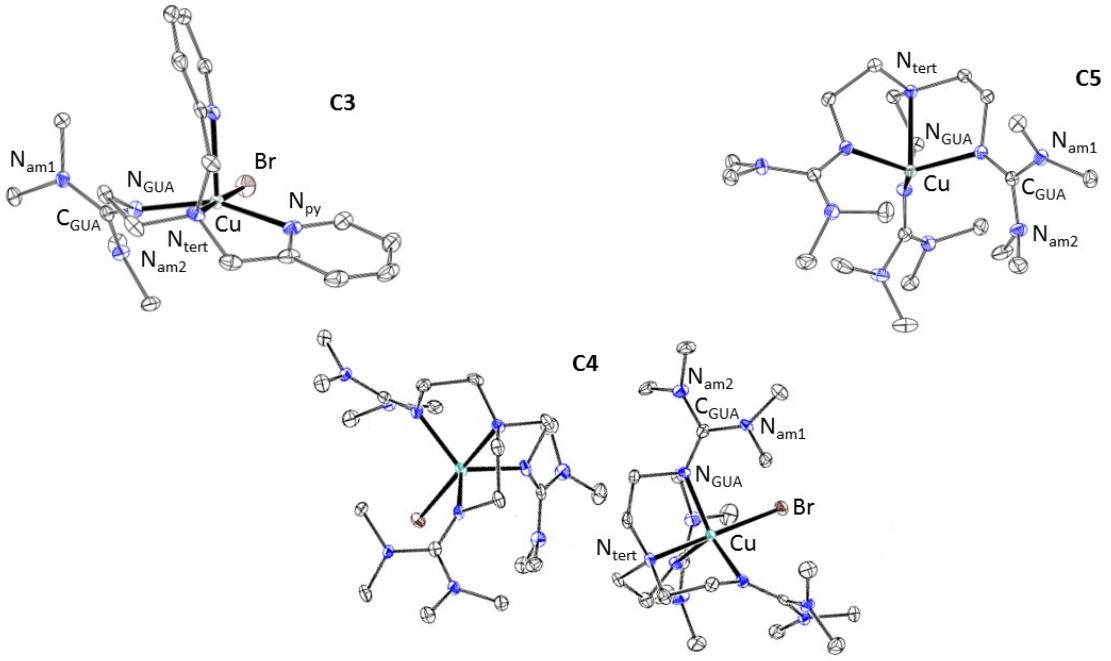

Fig. S2: Molecular structures of the cationic complex units of [Cu(TMG-uns-penp)Br]Br·MeCN (**C3**), [Cu(TMG$_3$tren)Br]Br (**C4**) and of the complex [Cu(TMG$_3$tren)]Br·toluene (**C5**) in the solid state (ellipsoids drawn at the 50% probability level). H atoms, not coordinating anions and solvent molecules are omitted for clarity.

Table S2: Crystallographic data and parameters of the Cu(II) complexes **C3**, **C4** and **C5**.

Complex/Ligand	**C3**	**C4**	**C5**
Empirical formula	$C_{21}H_{31}Br_2CuN_7$	$C_{21}H_{48}Br_2CuN_{10}$	$C_{21}H_{48}BrCuN_{10}$ [+C_7H_8]
Formula mass [g mol^{-1}]	604.89	664.05	584.14
Crystal size [mm]	0.26 x 0.23 x 0.20	0.26 x 0.25 x 0.23	0.21 x 0.15 x 0.12
T [K]	100(2)	100(2)	100(2)
Crystal system	Monoclinic	Monoclinic	Trigonal
Space group	$P2_1/c$	$P2_1/n$	$R\bar{3}$
a [Å]	14.006(3)	17.874(4)	11.8799(17)
b [Å]	14.715(3)	18.131(4)	11.8799(17)
c [Å]	12.068(2)	17.985(4)	35.794(7)
α [°]	90	90	90
β [°]	90.33(3)	81.20(3)	90
γ [°]	90	90	120
V [Å^3]	2487.2(8)	5827(2)	4374.9(15)
Z	4	8	6
$\rho_{calcd.}$ [g cm^{-3}]	1.615	1.514	1.330
μ [mm^{-1}]	4.114	3.521	2.146
λ [Å]	0.71073	0.71073	0.71073
F(000)	1220	2744	1848
hkl range	-17/17, -18/17, -11/14	-19/22, -23/23, -21/22	-18/18, -18/18, -56/29
Reflections collected	49459	108428	33104
Independent reflections	4873	12711	3801
$R_{int.}$	0.0331	0.1345	0.0716
No. parameters	285	637	104
R_1 [I $\geq 2\sigma(I)$]	0.0422	0.0475	0.0359
wR_2 (all data)	0.1206	0.1135	0.0818
Goodness-of-fit	1.054	1.085	1.023
$\Delta\rho_{fin}$ max/min [eÅ^{-3}]	1.069/-2.027	1.174/-0.820	0.536/-0.525

Table S3: Key bond lengths, angles and geometrical factors for both crystallographic independent molecules in the asymmetric unit of [Cu(TMG$_3$tren)Br]Br (**C4**).

Complex	**C4**	
	Bond lengths [Å]	
Cu-N_{ax}	2.112(3); N_{ax} = N_{tert}	2.113(3); N_{ax} = N_{tert}
Cu-N_{eq} (1)	2.061(3); N_{eq} = N_{GUA}	2.110(3); N_{eq} = N_{GUA}
Cu-N_{eq} (2)	2.065(3); N_{eq} = N_{GUA}	2.100(3); N_{eq} = N_{GUA}
Cu-N_{eq} (3)	2.138(3); N_{eq} = N_{GUA}	2.097(3); N_{eq} = N_{GUA}
Cu-X	2.447(1); X = Br	2.440(1); X = Br
C_{GUA}=N_{GUA}	1.311 (av.)	1.309 (av.)
C_{GUA}-N_{am1}	1.361 (av.)	1.376 (av.)
C_{GUA}-N_{am2}	1.360 (av.)	1.366 (av.)
	Bond angles [°]	
N_{ax}-Cu-X	179.4(1)	179.6(1)
N_{eq} (1)-Cu-X	98.8(1)	98.7(1)
N_{ax}-Cu-N_{eq} (1)	81.8(2)	81.6(2)
N_{ax}-Cu-N_{eq} (2)	82.3(2)	82.0(2)
N_{ax}-Cu-N_{eq} (3)	81.8(2)	81.9(2)
N_{eq} (1)-Cu-N_{eq} (2)	122.3(2)	119.5(2)
N_{eq} (1)-Cu-N_{eq} (3)	113.1(2)	115.7(2)
N_{eq} (2)-Cu-N_{eq} (3)	118.8(2)	118.8(2)
	Geometrical factors	
τ_5[a]	1.01	1.00
ρ[b]	0.96	0.96

[a] $\tau_5 = \frac{(\alpha - \beta)}{60°}$. Ideal square pyramidal complexes generate a τ_5 value of 0 where ideal trigonal bipyramidal complexes generate a τ_5 value of of 1.[5]

[b] $\rho = \frac{2a}{(b + c)}$ with a = d(C_{GUA}=N_{GUA}) and b and c = d(C_{GUA}-N_{am}).[6]

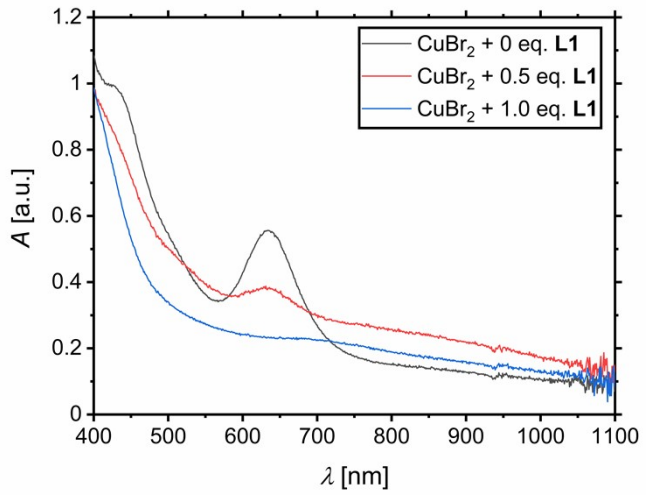

Fig. S3: UV/Vis spectra for 5 mM $CuBr_2$ in MeCN with 0 eq., 0.5 eq. or 1 eq. of TMG-4NMe_2uns-penp (**L1**).

UV/Vis spectra

EPR

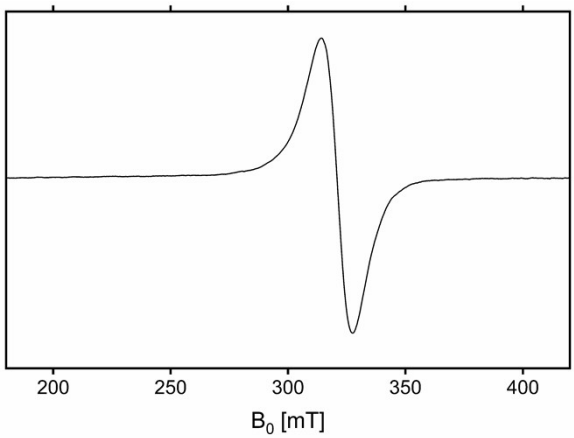

Fig. S4: Experimental X-band EPR spectrum of a frozen 5 mM **C1** complex solution in MeCN at 77 K.

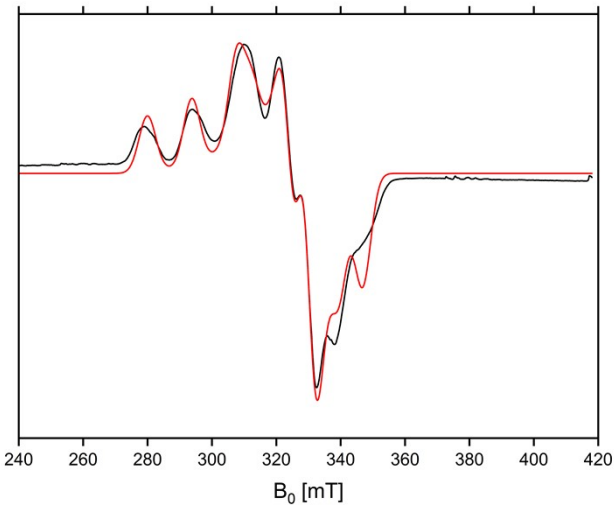

Fig. S5: Simulated and experimental X-band EPR spectra of frozen 5 mM **C1** complex solution in MeCN at 77 K.

Cyclic voltammogramms

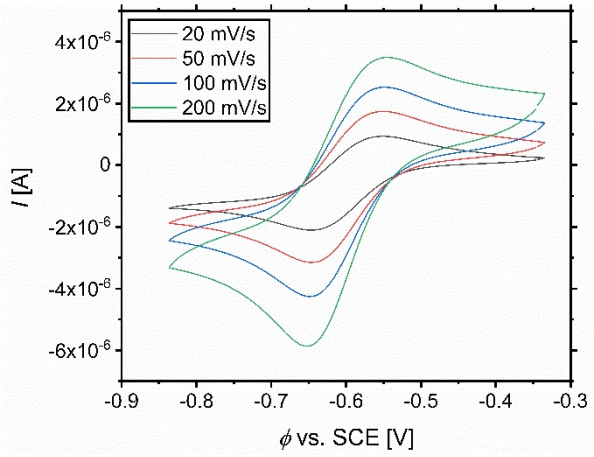

Fig. S6: Cyclic voltammograms with various scan rates of the $Cu^{I}L/Cu^{II}L$ couple starting from a 1 mM [Cu(TMG-4NMe$_2$uns-penp)Cl]Cl (**C2**) complex solution in MeCN.

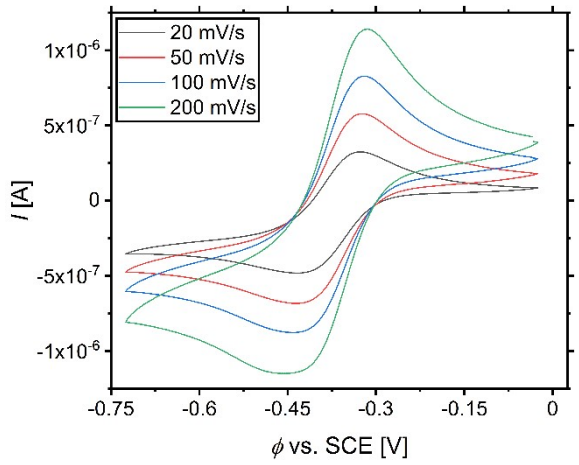

Fig. S7: Cyclic voltammograms with various scan rates of the $Cu^{I}L/Cu^{II}L$ couple starting from a 1 mM [Cu(TMG-4NMe$_2$uns-penp)](OTf)$_2$ complex solution in MeCN.

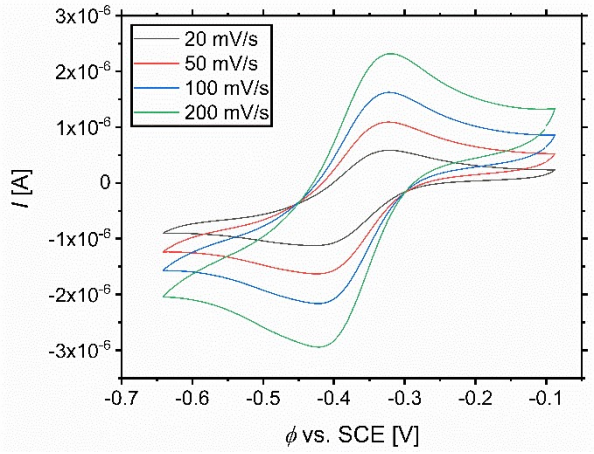

Fig. S8: Cyclic voltammograms with various scan rates of the $Cu^{I}L/Cu^{II}L$ couple starting from a 1 mM [Cu(TMG-uns-penp)Br]Br (**C3**) complex solution in MeCN.

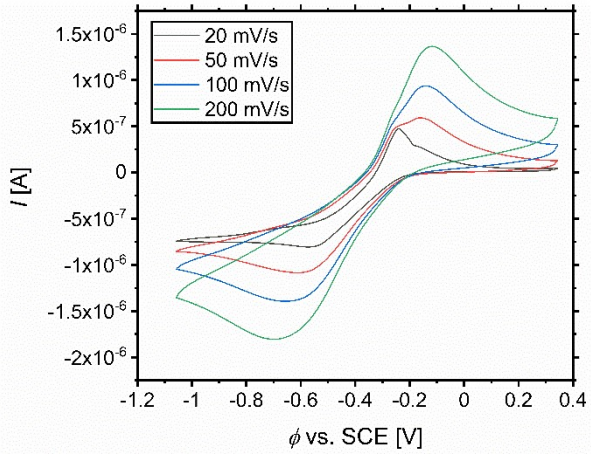

Fig. S9: Cyclic voltammograms with various scan rates of the $Cu^{I}L/Cu^{II}L$ couple starting from a 1 mM [Cu(TMG_3tren)Br]Br (**C4**) complex solution in MeCN.

Table S4 Additional data and parameters to the cyclic voltammograms of the $Cu^{I}L/Cu^{II}L$ couple using **L1** starting from 1 mM copper(II) bromide complex solution (**C1**) in MeCN.

	20 mV/s	50 mV/s	100 mV/s	200 mV/s
E_{ox} vs. SCE [V]	-0.437	-0.433	-0.429	-0.423
E_{red} vs. SCE [V]	-0.522	-0.526	-0.528	-0.532
$E_{1/2}$ vs. SCE [V]	-0.479	-0.479	-0.478	-0.477
ΔE [V]	0.085	0.093	0.099	0.109
I_{ox} [A]	6.47×10^{-7}	9.32×10^{-7}	1.22×10^{-6}	1.59×10^{-6}
I_{red} [A]	-6.47×10^{-7}	-9.81×10^{-7}	-1.35×10^{-6}	-1.83×10^{-6}
I_{red}/I_{ox}	-1.01	-1.05	-1.10	-1.15
Current function (ox) [µA $V^{-0.5}$ $s^{0.5}$ $mmol^{-1}$ l]	4.53×10^{-6}	4.17×10^{-6}	3.87×10^{-6}	3.56×10^{-6}
Current function (red) [µA $V^{-0.5}$ $s^{0.5}$ $mmol^{-1}$ l]	-4.57×10^{-6}	-4.39×10^{-6}	-4.25×10^{-6}	-4.09×10^{-6}

Table S5 Additional data and parameters to the cyclic voltammograms of the $Cu^{I}L/Cu^{II}L$ couple using **L1** starting from 1 mM copper(II) chloride complex solution (**C2**) in MeCN.

	20 mV/s	50 mV/s	100 mV/s	200 mV/s
E_{ox} vs. SCE [V]	-0.561	-0.561	-0.561	-0.561
E_{red} vs. SCE [V]	-0.636	-0.638	-0.640	-0.646
$E_{1/2}$ vs. SCE [V]	-0.599	-0.600	-0.601	-0.604
ΔE [V]	0.075	0.077	0.079	0.085
I_{ox} [A]	1.47×10^{-6}	2.18×10^{-6}	2.83×10^{-6}	3.59×10^{-6}
I_{red} [A]	-1.46×10^{-6}	-2.35×10^{-6}	-3.28×10^{-6}	-4.56×10^{-6}
I_{red}/I_{ox}	-0.99	-1.08	-1.16	-1.27
Current function (ox) [µA $V^{-0.5}$ $s^{0.5}$ $mmol^{-1}$ l]	1.04×10^{-5}	9.7×10^{-6}	8.9×10^{-6}	8.02×10^{-6}
Current function (red) [µA $V^{-0.5}$ $s^{0.5}$ $mmol^{-1}$ l]	-1.03×10^{-5}	-1.05×10^{-5}	-1.04×10^{-5}	-1.02×10^{-5}

Table S6 Additional data and parameters to the cyclic voltammograms of the $Cu^{I}L/Cu^{II}L$ couple using **L1** starting from 1 mM copper(II) triflate complex solution in MeCN.

	20 mV/s	50 mV/s	100 mV/s	200 mV/s
E_{ox} vs. SCE [V]	-0.334	-0.328	-0.324	-0.320
E_{red} vs. SCE [V]	-0.418	-0.418	-0.422	-0.418
$E_{1/2}$ vs. SCE [V]	-0.376	-0.373	-0.373	-0.369
ΔE [V]	0.083	0.089	0.097	0.097
I_{ox} [A]	4.37×10^{-7}	6.74×10^{-7}	9.10×10^{-7}	1.22×10^{-6}
I_{red} [A]	-3.72×10^{-7}	-5.53×10^{-7}	-7.27×10^{-7}	-9.37×10^{-7}
I_{red}/I_{ox}	-1.17	-1.21	-1.25	-1.30
Current function (ox) [µA $V^{-0.5}$ $s^{0.5}$ $mmol^{-1}$ l]	3.01×10^{-6}	3.02×10^{-6}	2.88×10^{-6}	2.72×10^{-6}
Current function (red) [µA $V^{-0.5}$ $s^{0.5}$ $mmol^{-1}$ l]	-2.63×10^{-6}	-2.47×10^{-6}	-2.30×10^{-6}	-2.10×10^{-6}

Table S7 Additional data and parameters to the cyclic voltammograms of the $Cu^{I}L/Cu^{II}L$ couple using **L2** starting from 1 mM copper(II) bromide complex solution in MeCN.

	20 mV/s	50 mV/s	100 mV/s	200 mV/s
E_{ox} vs. SCE [V]	-0.330	-0.332	-0.332	-0.332
E_{red} vs. SCE [V]	-0.410	-0.408	-0.410	-0.410
$E_{1/2}$ vs. SCE [V]	-0.370	-0.370	-0.371	-0.371
ΔE [V]	0.079	0.075	0.077	0.077
I_{ox} [A]	8.19×10^{-7}	1.27×10^{-6}	1.73×10^{-6}	2.33×10^{-6}
I_{red} [A]	-7.31×10^{-7}	-1.14×10^{-6}	-1.59×10^{-6}	-2.25×10^{-6}
I_{red}/I_{ox}	-0.89	-0.90	-0.924	-0.966
Current function (ox) [µA $V^{-0.5}$ $s^{0.5}$ $mmol^{-1}$ l]	5.79×10^{-6}	5.66×10^{-6}	5.46×10^{-6}	5.20×10^{-6}
Current function (red) [µA $V^{-0.5}$ $s^{0.5}$ $mmol^{-1}$ l]	-5.17×10^{-6}	-5.09×10^{-6}	-5.04×10^{-6}	-5.02×10^{-6}

Table S8 Additional data and parameters to the cyclic voltammograms of the $Cu^{I}L/Cu^{II}L$ couple using **L3** starting from 1 mM copper(II) bromide complex solution in MeCN.

	20 mV/s	50 mV/s	100 mV/s	200 mV/s
E_{ox} vs. SCE [V]	-0.241	-0.172	-0.154	-0.132
E_{red} vs. SCE [V]	-0.543	-0.568	-0.595	-0.630
$E_{1/2}$ vs. SCE [V]	-0.392	-0.370	-0.374	-0.381
ΔE [V]	0.302	0.397	0.440	0.497
I_{ox} [A]	8.11×10^{-7}	8.19×10^{-7}	1.09×10^{-6}	1.39×10^{-6}
I_{red} [A]	-4.80×10^{-7}	-6.75×10^{-7}	-8.58×10^{-7}	-1.06×10^{-6}
I_{red}/I_{ox}	-0.59	-0.82	-0.78	-0.76
Current function (ox) [µA $V^{-0.5}$ $s^{0.5}$ $mmol^{-1}$ l]	5.73×10^{-6}	3.66×10^{-6}	3.44×10^{-6}	3.11×10^{-6}
Current function (red) [µA $V^{-0.5}$ $s^{0.5}$ $mmol^{-1}$ l]	-3.39×10^{-6}	-3.01×10^{-6}	-2.71×10^{-6}	-2.36×10^{-6}

NMR spectra

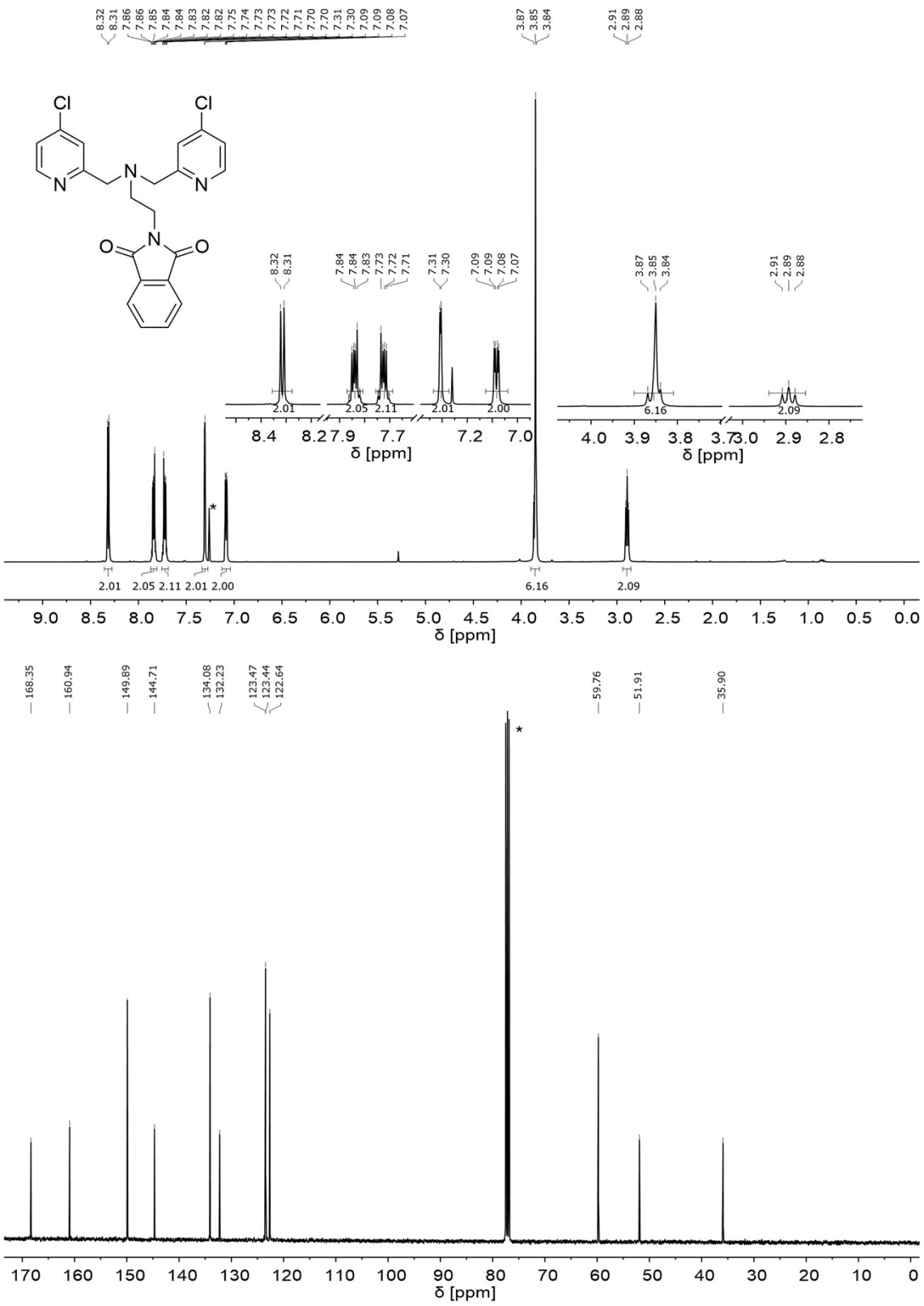

Fig. S10: ^{1}H-NMR (top) and ^{13}C-NMR (bottom) spectrum for 2-(2-(bis((4-chloropyridin-2-yl)methyl)amino)ethyl)isoindoline-1,3-dione (**3**) in $CDCl_3$. *: $CDCl_3$.

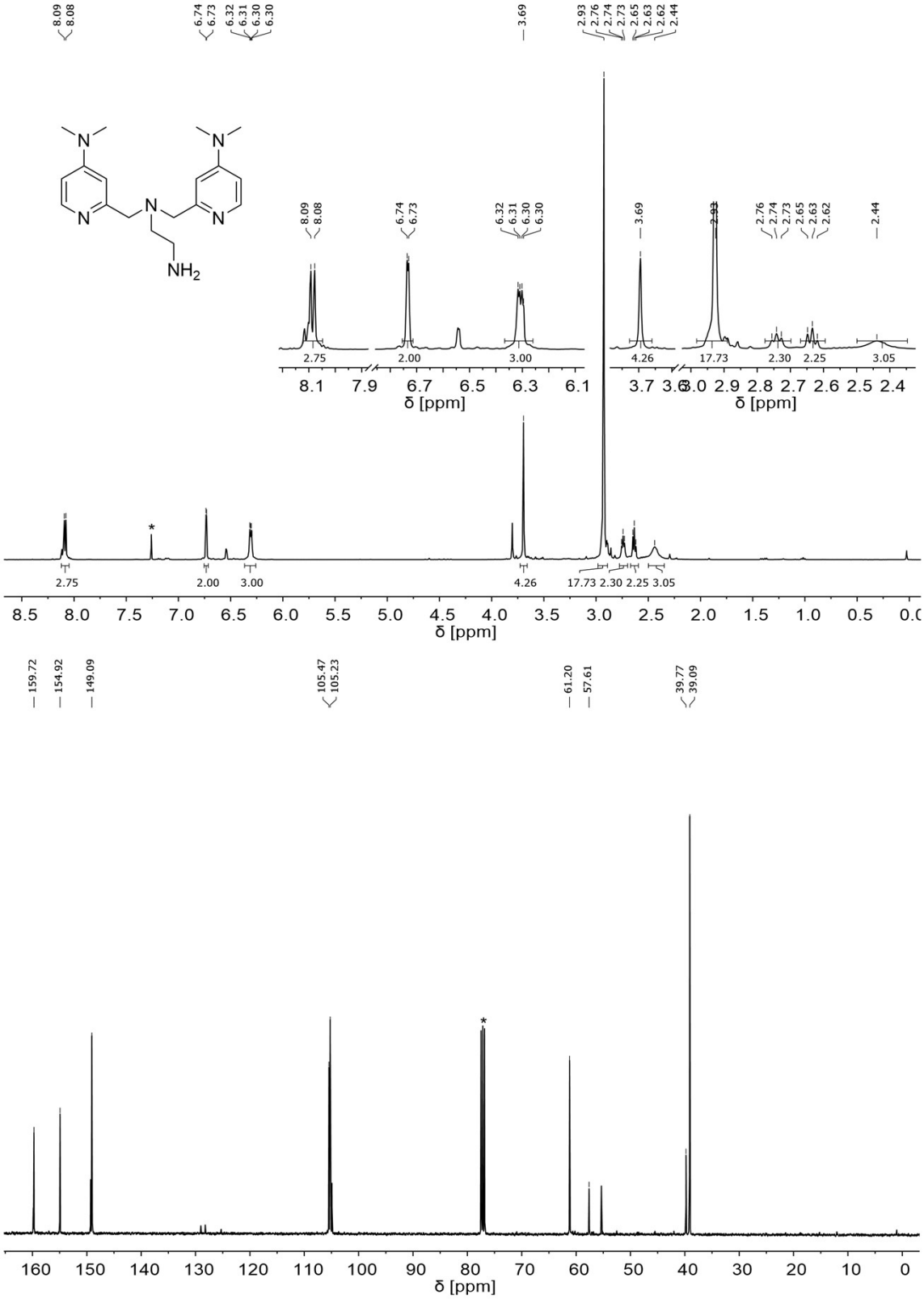

Fig. S11: ^{1}H-NMR (top) and ^{13}C-NMR (bottom) spectrum for N^{1},N^{1}-bis((4-(dimethylamino)pyridin-2-yl)methyl)ethane-1,2-diamine (**4**) in $CDCl_3$. *: $CDCl_3$.

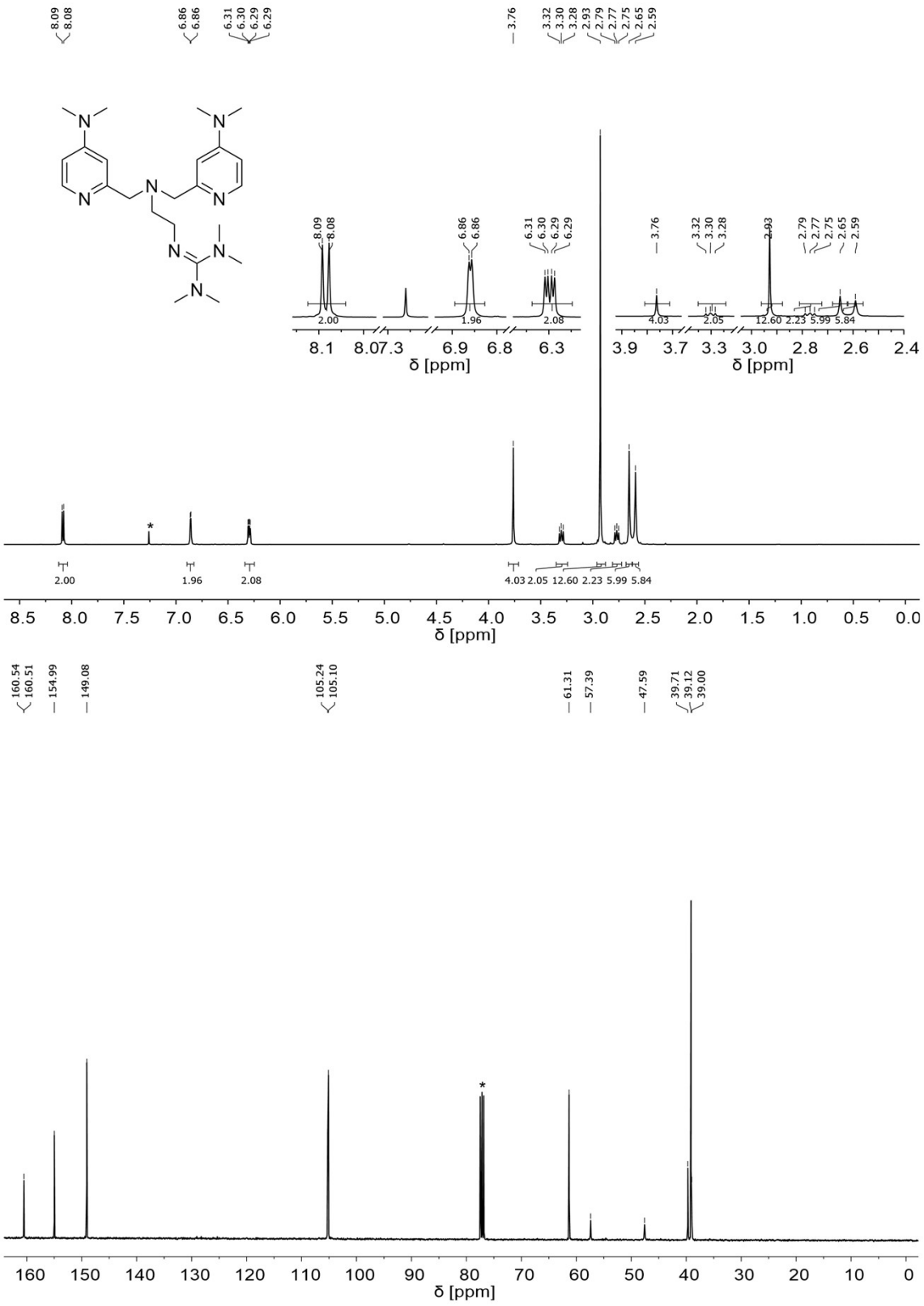

Fig. S12: ^{1}H-NMR (top) and ^{13}C-NMR (bottom) spectrum for TMG-4NMe$_2$uns-penp (**L1**) in $CDCl_3$. *: $CDCl_3$.

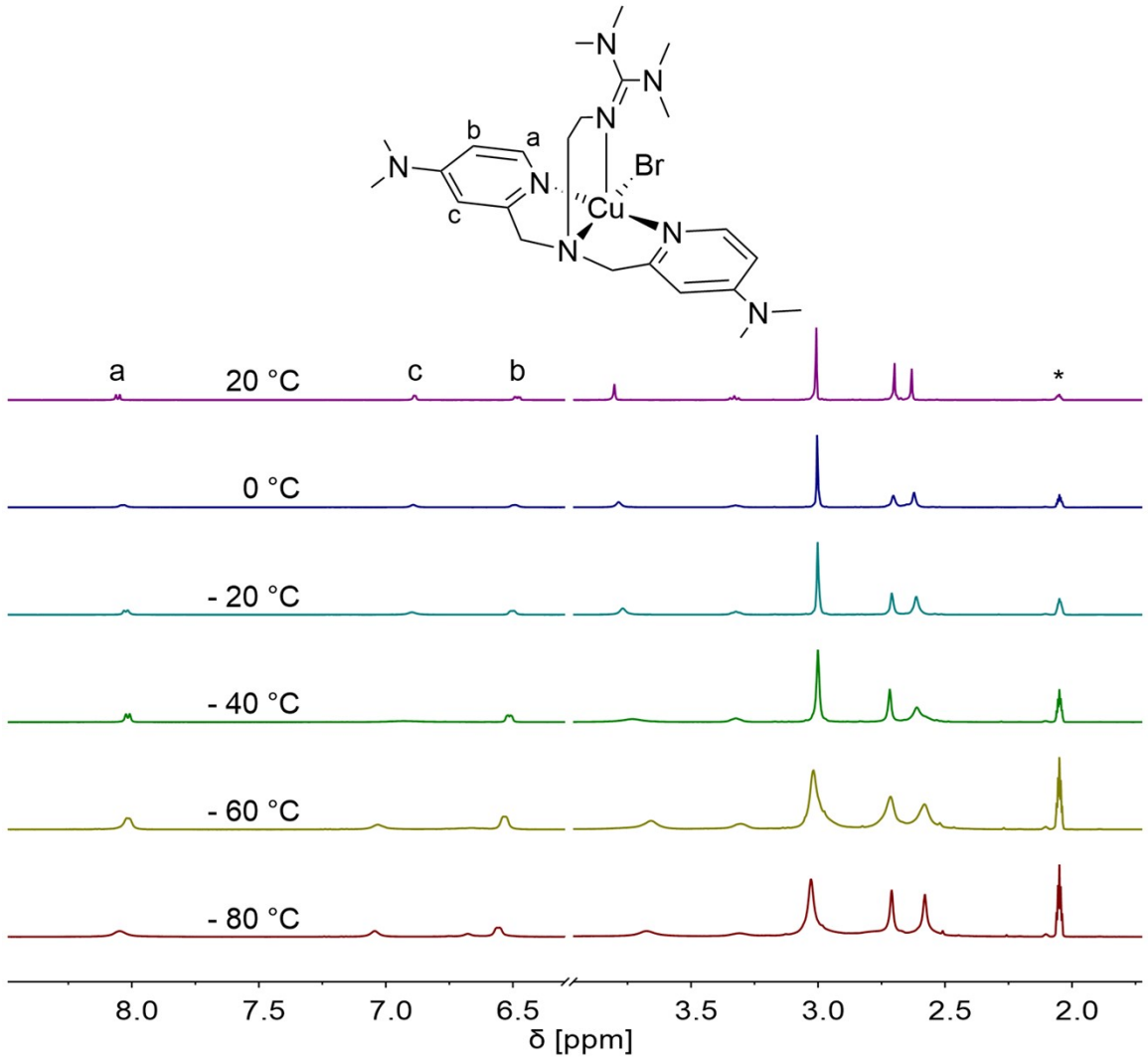

Fig. S13: Variable-temperature ^{1}H-NMR spectra of the **L1** based CuBr complex in d_6-acetone at a molar ratio of [CuBr]:[L1] = 1:3. *: d_6-acetone.

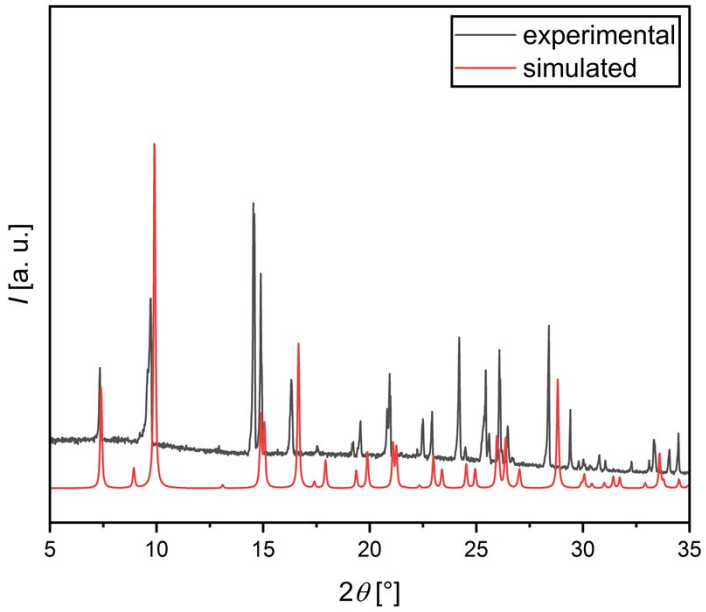

Fig. S14: Experimental and simulated PXRD spectra of **C5**.

PXRD spectrum

DFT calculations of the complex cations

Table S9: XRD and DFT calculated key bond lengths, angles and geometrical factors of the copper(II) deactivator complexes in **C1**, **C3**, **C4**, [Cu(TPMA^{NMe2})Br]Br[7] and [Cu(TPMA)Br]Br.[8,9]

DFT					
Complex	**Cation in C1**	**Cation in C3**	**Cation in C4**	[Cu(TPMA^{NMe2})Br]$^+$	[Cu(TPMA)Br]$^+$
Bond lengths [Å]					
Cu-N_{ax}	2.224; N_{ax} = N_{GUA}	2.231; N_{ax} = N_{py}	2.136; N_{ax} = N_{tert}	2.070; N_{ax} = N_{tert}	2.066; N_{ax} = N_{tert}
Cu-$N_{b/eq}$ (1)	2.107; N_b = N_{tert}	2.122; N_b = N_{tert}	2.092; N_{eq} = N_{GUA}	2.064; N_{eq} = N_{py}	2.072; N_{eq} = N_{py}
Cu-$N_{b/eq}$ (2)	2.002; N_b = N_{py}	1.972; N_b = N_{GUA}	2.092; N_{eq} = N_{GUA}	2.064; N_{eq} = N_{py}	2.073; N_{eq} = N_{py}
Cu-$N_{b/eq}$ (3)	2.009; N_b = N_{py}	2.025; N_b = N_{py}	2.092; N_{eq} = N_{GUA}	2.064; N_{eq} = N_{py}	2.072 N_{eq} = N_{py}
Cu-Br	2.455	2.443	2.473	2.423	2.405
Bond angles [°]					
N_{ax}-Cu-Br	113.5	97.3	180.0	180.0	179.9
$N_{b/eq}$ (1)-Cu-Br	163.8	175.9	98.2	99.3	99.3
N_{ax}-Cu-$N_{b/eq}$ (1)	82.5	79.4	81.8	80.7	80.7
N_{ax}-Cu-$N_{b/eq}$ (2)	104.9	96.3	81.8	80.7	80.7
N_{ax}-Cu-$N_{b/eq}$ (3)	88.0	104.9	81.8	80.7	80.7
$N_{b/eq}$ (1)-Cu-$N_{b/eq}$ (2)	81.2	83.2	118.0	117.3	117.6
$N_{b/eq}$ (1)-Cu-$N_{b/eq}$ (3)	82.3	80.3	118.0	117.3	117.3
$N_{b/eq}$ (2)-Cu-$N_{b/eq}$ (3)	157.5	150.1	118.0	117.7	117.5
Geometrical factor					
τ_5[a]	0.11	0.43	1.03	1.04	1.03
XRD					
Complex	**C1**	**C3**	**C4**	[Cu(TPMA^{NMe2})Br]Br	[Cu(TPMA)Br]Br
Bond lengths [Å]					
Cu-N_{ax}	2.188(2); N_{ax} = N_{GUA}	2.231(4); N_{ax} = N_{py}	2.112(3); N_{ax} = N_{tert}	2.047(3); N_{ax} = N_{tert}	2.066; N_{ax} = N_{tert}
Cu-$N_{b/eq}$ (1)	2.088(2); N_b = N_{tert}	2.082(4); N_b = N_{tert}	2.061(3); N_{eq} = N_{GUA}	2.051(2); N_{eq} = N_{py}	2.072; N_{eq} = N_{py}
Cu-$N_{b/eq}$ (2)	2.010(2); N_b = N_{py}	1.970(4); N_b = N_{GUA}	2.065(3); N_{eq} = N_{GUA}	2.108(3); N_{eq} = N_{py}	2.073; N_{eq} = N_{py}
Cu-$N_{b/eq}$ (3)	2.020(2); N_b = N_{py}	2.031(4); N_b = N_{py}	2.138(3); N_{eq} = N_{GUA}	2.046(3); N_{eq} = N_{py}	2.072 N_{eq} = N_{py}
Cu-Br	2.438(1)	2.394(1)	2.447(1)	2.390(1)	2.405
Bond angles [°]					
N_{ax}-Cu-Br	101.9(1)	99.4(1)	179.4(1)	179.9(1)	180.0(1)
$N_{b/eq}$ (1)-Cu-Br	174.7(1)	177.2(1)	98.8(1)	98.6(1)	99.1(1)
N_{ax}-Cu-$N_{b/eq}$ (1)	83.1(1)	80.1(2)	81.8(2)	80.6(1)	80.9(1)
N_{ax}-Cu-$N_{b/eq}$ (2)	107.7(1)	95.6(2)	82.3(2)	80.6(1)	80.9(1)
N_{ax}-Cu-$N_{b/eq}$ (3)	92.5(1)	102.8(2)	81.8(2)	81.4(1)	80.9(1)
$N_{b/eq}$ (1)-Cu-$N_{b/eq}$ (2)	82.2(1)	84.0(2)	122.3(2)	126.6(1)	117.5(1)
$N_{b/eq}$ (1)-Cu-$N_{b/eq}$ (3)	82.2(1)	80.3(2)	113.1(2)	116.3(1)	117.5(1)
$N_{b/eq}$ (2)-Cu-$N_{b/eq}$ (3)	152.6(1)	153.3(2)	118.8(2)	109.4(1)	117.5(1)
Geometrical factor					
τ_5[a]	0.37	0.36	1.01	0.89	1.00
RMSD vs. SCXRD [Å]	0.3358	0.1604	0.0906	0.1416	0.0290

[a] $\tau_5 = \frac{(\alpha - \beta)}{60°}$. Ideal square-pyramidal complexes generate a τ_5 value of 0, whereas ideal trigonal-bipyramidal complexes generate a τ_5 value of 1.[5]

In the DFT optimisation calculation of [Cu(TMG4NMe$_2$unspenp)Br]$^+$ (cation in **C1**), a minimum structure with a N_{tert}-Cu-Br bond angle of 163.8° was found which is contrary to the N_{tert}-Cu-Br bond angle of 174.8° in the solid state. To verify the found minimum of the DFT optimisation calculation, a Conformer-Rotamer Ensemble Sampling Tool (CREST) calculation was performed.[10,11] The applied theory level was GFN2-xTB.[12,13] To prevent topology changes in the coordination geometry of the CuN_4 unit, constraints on the copper center and the N donors were applied. The minimum structure of the CREST calculation confirms the smaller N_{tert}-Cu-Br bond angle found in the DFT optimisation calculation since the CREST calculation found a N_{tert}-Cu-Br bond angle of 157.3°. An analogous procedure was applied to complex **C3** to show that the structure obtained describes the true minimum of the DFT optimisation calculation and thus proves the exchange in the coordination of the N donors depending on the dimethylamine substituents on the pyridene.

Table S10: XRD and DFT calculated key bond lengths, angles and geometrical factors of the complex cations in **C2** and **C5**.

	DFT		XRD	
Complex	**Cation in C2**	**Cation in C5**	**Cation in C2**	**Cation in C5**
Bond lengths [Å]				
Cu-N_{ax}	2.232; $N_{ax} = N_{GUA}$	2.216; $N_{ax} = N_{tert}$	2.201(2); $N_{ax} = N_{GUA}$	2.200(2); $N_{ax} = N_{tert}$
Cu-$N_{b/eq}$ (1)	2.105; $N_b = N_{tert}$	2.038; $N_b = N_{GUA}$	2.089(2); $N_b = N_{tert}$	2.053(2); $N_b = N_{GUA}$
Cu-$N_{b/eq}$ (2)	2.000; $N_b = N_{py}$	2.038; $N_b = N_{GUA}$	2.009(2); $N_b = N_{py}$	2.053(2); $N_b = N_{GUA}$
Cu-$N_{b/eq}$ (3)	2.008; $N_b = N_{py}$	2.037; $N_b = N_{GUA}$	1.999(2); $N_b = N_{py}$	2.053(2); $N_b = N_{GUA}$
Cu-Cl	2.297	-	2.282(1)	-
Bond angles [°]				
N_{ax}-Cu-Br	111.5	-	102.7(1)	-
$N_{b/eq}$ (1)-Cu-Br	166.2	-	174.5(1)	-
N_{ax}-Cu-$N_{b/eq}$ (1)	82.2	84.3	82.7(1)	84.1(1)
N_{ax}-Cu-$N_{b/eq}$ (2)	88.4	84.3	91.7(1)	84.1(1)
N_{ax}-Cu-$N_{b/eq}$ (3)	105.5	84.2	108.0(1)	84.1(1)
$N_{b/eq}$ (1)-Cu-$N_{b/eq}$ (2)	82.4	119.0	82.5(1)	119.0(1)
$N_{b/eq}$ (1)-Cu-$N_{b/eq}$ (3)	81.3	119.0	82.0(1)	119.0(1)
$N_{b/eq}$ (2)-Cu-$N_{b/eq}$ (3)	156.9	119.0	153.0(1)	119.0(1)
Geometrical factors				
τ_4[a]/THC_{DA}[b]	-	0.87/-15.8	-	0.86/-16.2
τ_5[c]	0.16	-	0.36	-

[a] $\tau_4 = \frac{360° - (\alpha + \beta)}{141°}$. Ideal square-planar complexes generate a τ_4 value of 0; whereas ideal tetrahedral complexes generate a τ_4 value of 1.[14]

[b] $THC_{DA} = \left(1 - \frac{\Sigma n = 1 - 6\,|109.5° - \theta n|}{90°}\right) \times 100$ .The THC_{DA} value reaches 100 for ideal tetrahedral complexes and 0 for ideal trigonal-pyramidal complexes.[14]

[c] $\tau_5 = \frac{(\alpha - \beta)}{60°}$. Ideal square-pyramidal complexes generate a τ_5 value of 0, whereas ideal trigonal-bipyramidal complexes generate a τ_5 value of 1.[5]

Table S11: Calculated NBO charges and charge-transfer energies of selected atoms and bonds for the copper(II) deactivator complex cations in **C1**, **C3**, **C4**, [Cu(TPMA^{NMe2})Br]Br and [Cu(TPMA)Br]Br (NBO7 to.0; TPSSh/def2-TZVP and PCM solvent model for acetonitrile and the empirical dispersion correction with Becke-Johnson damping).

Complex cation in	**C1**	**C3**	**C4**	[Cu(TPMA^{NMe2})Br]Br	[Cu(TPMA)Br]Br
NBO charges [e units]					
Cu	1.25	1.23	1.28	1.25	1.24
N_{ax}	-0.69; $N_{ax} = N_{GUA}$	-0.53; $N_{ax} = N_{py}$	-0.44; $N_{ax} = N_{tert}$	-0.41; $N_{ax} = N_{tert}$	-0.41; $N_{ax} = N_{tert}$
$N_{b/eq}$ (1)	-0.44; $N_b = N_{tert}$	-0.43; $N_b = N_{tert}$	-0.71; $N_{eq} = N_{GUA}$	-0.59; $N_{eq} = N_{py}$	-0.53; $N_{eq} = N_{py}$
$N_{b/eq}$ (2)	-0.57; $N_b = N_{py}$	-0.70; $N_b = N_{GUA}$	-0.71; $N_{eq} = N_{GUA}$	-0.59; $N_{eq} = N_{py}$	-0.53; $N_{eq} = N_{py}$
$N_{b/eq}$ (3)	-0.57; $N_b = N_{py}$	-0.53; $N_b = N_{py}$	-0.71; $N_{eq} = N_{GUA}$	-0.59; $N_{eq} = N_{py}$	-0.53; $N_{eq} = N_{py}$
Br	-0.74	-0.73	-0.73	-0.72	-0.69
E_{CT} [kcal mol^{-1}]					
N_{ax} → Cu	20.6; $N_{ax} = N_{GUA}$	19.0; $N_{ax} = N_{py}$	32.6; $N_{ax} = N_{tert}$	45.8; $N_{ax} = N_{tert}$	47.7; $N_{ax} = N_{tert}$
$N_{b/eq}$ (1) → Cu	35.0; $N_b = N_{tert}$	36.0; $N_b = N_{tert}$	27.3; $N_{eq} = N_{GUA}$	37.1; $N_{eq} = N_{py}$	34.9; $N_{eq} = N_{py}$
$N_{b/eq}$ (2) → Cu	54.4; $N_b = N_{py}$	47.1; $N_b = N_{GUA}$	27.3; $N_{eq} = N_{GUA}$	37.1; $N_{eq} = N_{py}$	34.9; $N_{eq} = N_{py}$
$N_{b/eq}$ (3) → Cu	51.2; $N_b = N_{py}$	47.8; $N_b = N_{py}$	27.3; $N_{eq} = N_{GUA}$	36.9; $N_{eq} = N_{py}$	34.9; $N_{eq} = N_{py}$
$E_{CT,total}$	161.2	149.9	114.5	156.9	152.4
Br → Cu	89.8	98.5	79.9	115.7	142.9

Table S12: Calculated NBO charges and charge-transfer energies of selected atoms and bonds for the copper(II) deactivator complex cations in **C2** and **C5**. (NBO7 to.0; TPSSh/def2-TZVP and PCM solvent model for acetonitrile and the empirical dispersion correction with Becke-Johnson damping).

Complex cations in	**C2**	**C5**
NBO charges [e units]		
Cu	1.28	0.90
N_{ax}	-0.69; $N_{ax} = N_{GUA}$	-0.50; $N_{ax} = N_{tert}$
$N_{b/eq}$ (1)	-0.44; $N_b = N_{tert}$	-0.68; $N_b = N_{GUA}$
$N_{b/eq}$ (2)	-0.57; $N_b = N_{py}$	-0.68; $N_b = N_{GUA}$
$N_{b/eq}$ (3)	-0.57; $N_b = N_{py}$	-0.68; $N_b = N_{GUA}$
Cl	-0.76	-
E_{CT} [kcal mol^{-1}]		
N_{ax} → Cu	19.7; $N_{ax} = N_{GUA}$	4.1; $N_{ax} = N_{ret}$
$N_{b/eq}$ (1) → Cu	36.1; $N_b = N_{tert}$	21.1; $N_b = N_{GUA}$
$N_{b/eq}$ (2) → Cu	54.6; $N_b = N_{py}$	21.1; $N_b = N_{GUA}$
$N_{b/eq}$ (3) → Cu	51.1; $N_b = N_{py}$	21.1; $N_b = N_{GUA}$
$E_{CT,total}$	161.5	67.4
Cl → Cu	84.5	-

Polymerisations

ATRP

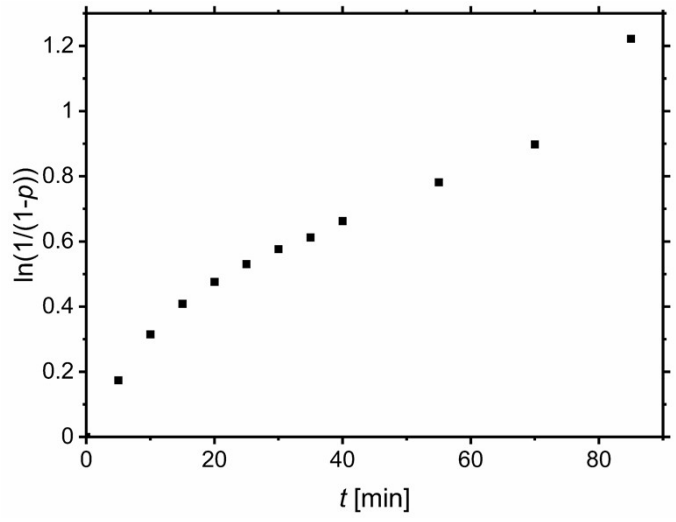

Fig. S15: Semilogarithmic plot of conversion vs. time for styrene ATRP with the CuBr/TMG-4NMe$_2$uns-penp catalyst system. Conditions: Styrene/EBiB/Cat. =

ICAR ATRP

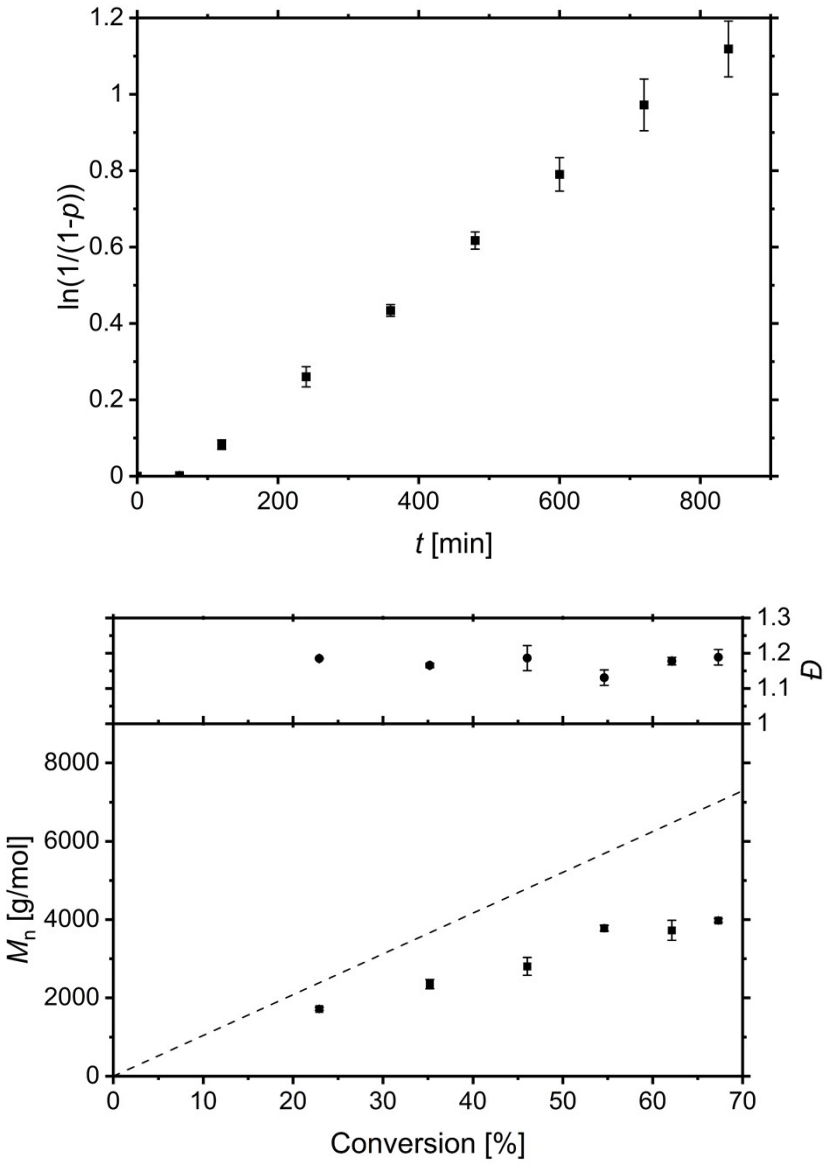

Fig. S16: Semilogarithmic plot of conversion vs. time (top) and plot of M_n/$Đ$ vs. conversion (bottom) for ICAR ATRP of styrene with the $CuBr_2$/**L3** catalyst system. Conditions: Styrene/ /EBiB/ Cat./AIBN = 100/1/0.1/1.5 in benzonitrile at 60 °C.

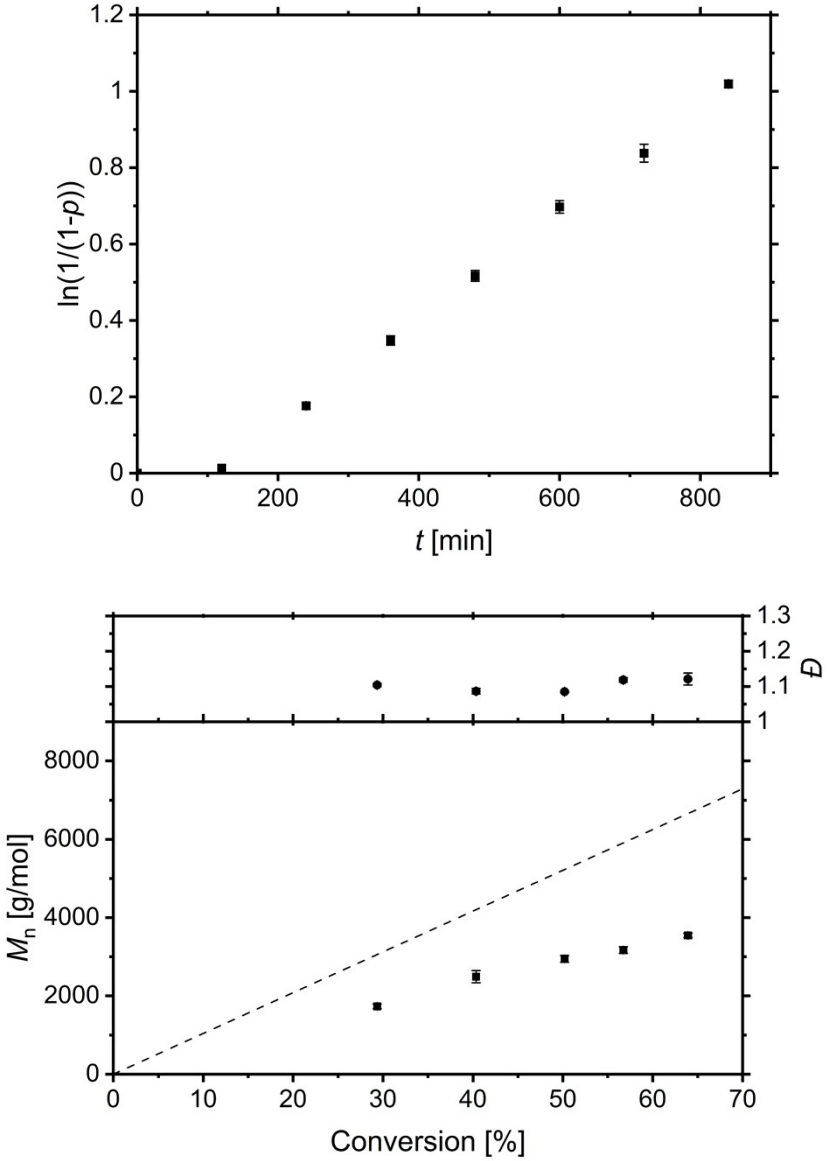

Fig. S17: Semilogarithmic plot of conversion vs. time (top) and plot of M_n/$Đ$ vs. conversion (bottom) for ICAR ATRP of styrene with the $CuBr_2$/TPMA catalyst system. Conditions: Styrene/ /EBiB/ Cat./AIBN = 100/1/0.1/1.5 in benzonitrile at 60 °C.

Ligand structures

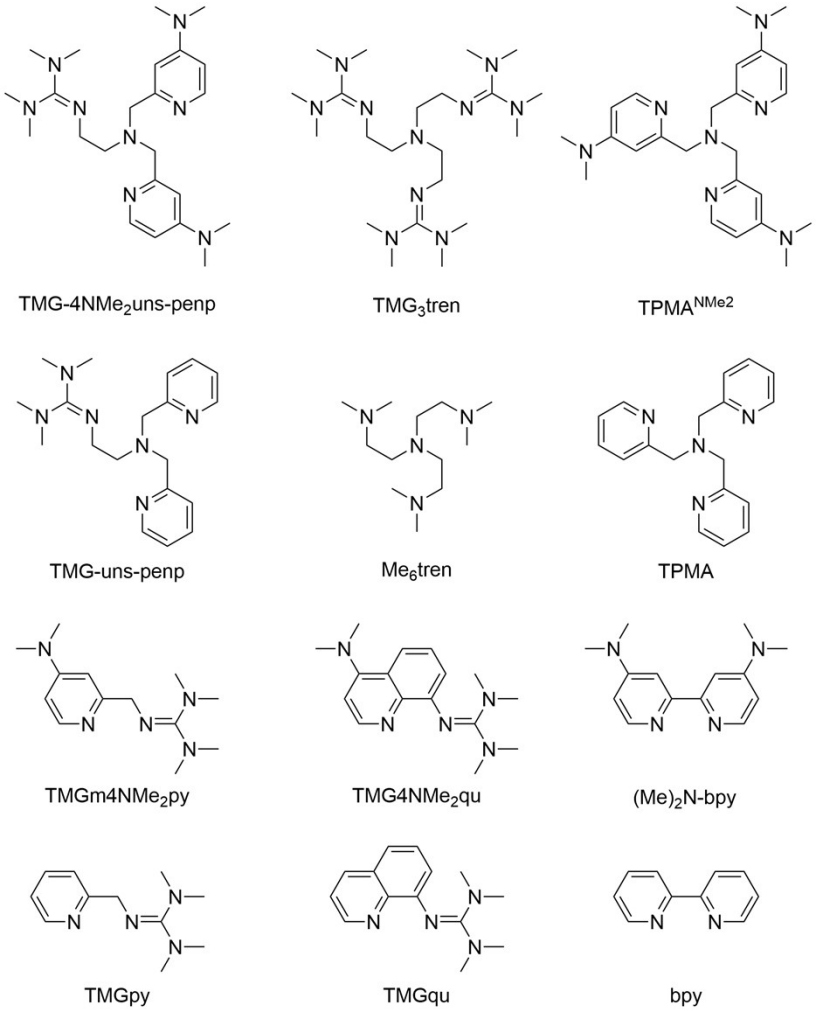

Fig. S18 Various ligand structures and their short names.

References

1 L. I. Manasieva, B. U. Maria, A. Prandi, L. Brasili, S. Franchini, *Synthesis* **2015**, *47*, 3767-3775.
2 R. L. Lucas, M. K. Zart, J. Murkerjee, T. N. Sorrell, D. R. Powell, A. S. Borovik, *J. Am. Chem. Soc.* **2006**, *128*, 15476-15489.
3 M. Mori, M. C. Dasso Lang, F. Saladini, N. Palombi, L. Kovalenko, D. De Forni, B. Poddesu, L. Friggeri, A. Giannini, S. Malancona, V. Summa, M. Zazzi, Y. Mely, M. Botta, *ACS Med. Chem. Lett.* **2019**, *10*, 463-468.
4 H. Fuchida, S. Tabata, N. Shindo, I. Takashima, Q. Leng, Y. Hatsuyama, I. Hamachi, A. Ojida, *Bull. Chem. Soc. Jpn.* **2015**, *88*, 784-791.
5 A. W. Addison, T. N. Rao, J. Reedijk, J. van Rijn, G. C. Verschoor, *J. Chem. Soc., Dalton Trans.* **1984**, 1349-1356.
6 V. Raab, K. Harms, J. Sundermeyer, B. Kovačević, Z. B. Maksić, *J. Org. Chem.* **2003**, *68*, 8790-8797.
7 T. G. Ribelli, M. Fantin, J.-C. Daran, K. F. Augustine, R. Poli, K. Matyjaszewski, *J. Am. Chem. Soc.* **2018**, *140*, 1525-1534.
8 W. T. Eckenhoff, S. T. Garrity, T. Pintauer, *Eur. J. Inorg. Chem.* **2008**, *2008*, 563-571.
9 W. T. Eckenhoff, T. Pintauer, *Inorg. Chem.* **2010**, *49*, 10617-10626.
10 P. Pracht, F. Bohle, S. Grimme, *Phys. Chem. Chem. Phys.* **2020**, *22*, 7169-7192.
11 C. Plett, S. Grimme, *Angew. Chem. Int. Ed.* **2023**, *62*, e202214477; *Angew. Chem.* **2023**, *135*, e202214477.
12 S. Grimme, *J. Chem. Theory Comput.* **2019**, *15*, 2847-2862.
13 S. Spicher, C. Plett, P. Pracht, A. Hansen, S. Grimme, *J. Chem. Theory Comput.* **2022**, *18*, 3174-3189.
14 L. Yang, D. R. Powell, R. P. Houser, *Dalton Trans.* **2007**, 955-964.